Identification of excited states in ^{119}Ba

J. F. Smith,[1,2,*] C. J. Chiara,[1] D. B. Fossan,[1] G. J. Lane,[1,†] J. M. Sears,[1] I. Thorslund,[1] H. Amro,[3] C. N. Davids,[3] R. V. F. Janssens,[3] D. Seweryniak,[3] I. M. Hibbert,[4,‡] R. Wadsworth,[4] I. Y. Lee,[5] A. O. Macchiavelli,[5] A. V. Afanasjev,[6,7] and I. Ragnarsson[8]

[1]*Department of Physics and Astronomy, State University of New York at Stony Brook, Stony Brook, New York 11794-3800*

[2]*Schuster Laboratory, The University of Manchester, Manchester, M13 9PL, United Kingdom*

[3]*Argonne National Laboratory, Argonne, Illinois 60439*

[4]*Department of Physics, University of York, Heslington, York, YO1 5DD, United Kingdom*

[5]*Nuclear Science Division, Lawrence Berkeley National Laboratory, Berkeley, California 94720*

[6]*Laboratory of Radiation Physics, Institute of Solid State Physics, University of Latvia, LV 2169, Miera str. 31, Salaspils, Latvia*

[7]*Physik Department T30, Technischen Universität München, D-85748 Garching, Germany*

[8]*Department of Mathematical Physics, Lund Institute of Technology, Box 118, S-22100 Lund, Sweden*

(Received 25 October 1999; published 23 March 2000)

Excited states have been identified in the very neutron-deficient ^{119}Ba nucleus. Two bands have been observed, which are likely to be based on $h_{11/2}$ and $(g_{7/2}d_{5/2})$ neutron orbitals. Despite this being the first observation of excited states in ^{119}Ba, the bands extend to $(75/2)\hbar$ and $(79/2)\hbar$, respectively. The bands have been assigned to ^{119}Ba using gamma-recoil and gamma–x-ray coincidences. Several quasiparticle alignments have been identified, involving neutron $(h_{11/2})^2$ and proton $(h_{11/2})^2$ aligned configurations. Furthermore, the bands show features which are reasonably consistent with smooth band termination at high spin. Theoretical results for ^{119}Ba are discussed within the framework of cranked Woods-Saxon and Nilsson-Strutinsky calculations.

PACS number(s): 21.10.Re, 23.20.Lv, 27.60.+j, 29.30.Kv

I. INTRODUCTION

The $Z=56$ barium nuclei represent one of the best examples of an isotopic chain in which to trace the evolution of nuclear structure with neutron number. With the exception of ^{119}Ba, excited states have been identified in every barium isotope from $A=118$ [1] to $A=148$ [2]. The neutron-deficient barium isotopes with $120<A<130$ have well-developed quadrupole deformations ($\beta_2=0.2$–0.3) and are easily produced in heavy-ion fusion evaporation reactions; these nuclei have therefore been very well studied in gamma-ray spectroscopy experiments. A wealth of data exist on collective and quasiparticle excitations in these nuclei [3–8], with many of these nuclei exhibiting multiple extended rotational bands. However, the barium isotopes with $A<120$ are not as easy to populate, and can be produced only with small cross sections in reactions involving neutron evaporation from the most-neutron-deficient compound nuclei achievable. Despite experimental difficulties, there is considerable motivation to study the most-neutron-deficient barium isotopes, as described below.

The structure of these nuclei is strongly influenced by the occupation of $h_{11/2}$ intruder orbitals for both protons and neutrons. The alignments of pairs of both $h_{11/2}$ neutrons and $h_{11/2}$ protons are predicted to occur [9,10] at similar frequencies (0.3–0.4 MeV/$\hbar$), with the precise frequency depending upon the deformation. The investigation of quasiparticle alignments is important for defining configurations via Pauli blocking arguments and for the study of nuclear shapes in odd-A nuclei. In addition, as a consequence of the small number of valence particles outside the $N=Z=50$ double shell closure, band termination effects are important. The phenomenon of smooth band termination [11,12] has been established for several years in the nuclei immediately above ^{100}Sn [13–21]. Smooth band termination describes the situation where all of the valence nucleons in the configuration of a collective rotational band gradually align their angular momenta with the axis of rotation, eventually resulting in a noncollective oblate terminating state. Once all of the nucleons are aligned, the available angular momentum is exhausted and the band terminates. Recently, some evidence has been presented for smooth band termination in $^{117-119}_{54}$Xe [22,23]. With the phenomenon firmly established in the tin ($Z=50$) to iodine ($Z=53$) isotopes, it is important to search for the effect further away from the double shell closure, where the collectivity might be generated by a different mechanism.

An experimental study of ^{119}Ba has been performed in order to investigate high-spin properties, such as quasiparticle alignments, in this very-neutron-deficient region and also to investigate smooth band-termination effects. The spectroscopy of barium isotopes with $A<120$ has only become possible with the advent of the third generation of detector arrays such as GAMMASPHERE [24]. This paper reports on the first observation and identification of excited states in ^{119}Ba;

*Corresponding author: Schuster Laboratory, The University of Manchester, Manchester, M13 9PL, UK; Tel: (44) 161 275 4155, Fax: (44) 161 275 5509.

Electronic address: jfs@mags.ph.man.ac.uk

†Present address: Nuclear Science Division, Lawrence Berkeley National Laboratory, Berkeley, CA 94720.

‡Present address: Oliver Lodge Laboratory, University of Liverpool, Liverpool, L69 7ZE, UK.

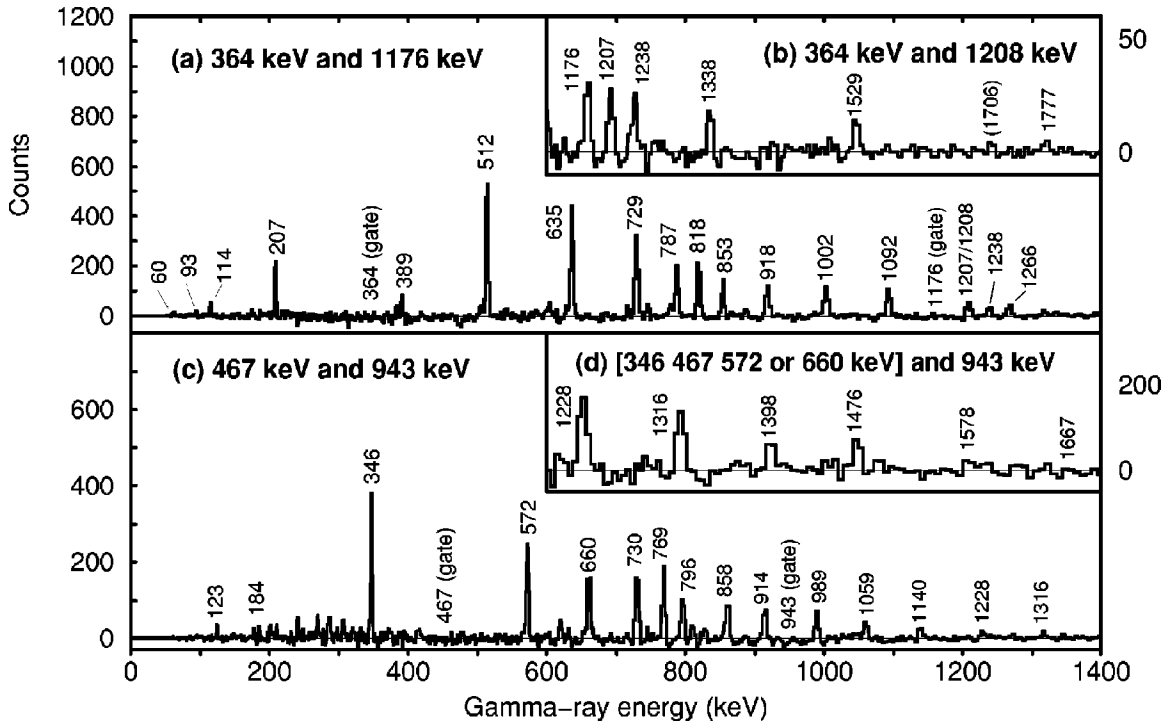

FIG. 1. Representative spectra from the GAMMASPHERE experiment. The spectra are projected from a cube by gating on the specified transitions. Panels (a) and (b) show transitions in the $\alpha=-1/2$ sequence of the $\nu(h_{11/2})$ band, and (c) and (d) show transitions in the $\alpha=-1/2$ sequence of the $\nu(g_{7/2}d_{5/2})$ band. The peaks are labeled with transition energies, given to the nearest keV, and all of the labeled peaks are transitions in ^{119}Ba. The transition at 1706 keV appears to be in coincidence with ^{119}Ba transitions, but has not been placed in the level scheme. The coincidence with the 389-keV transition in panel (a) presumably arises via weak unobserved $\Delta I=1M1/E2$ transitions.

the ^{64}Zn(^{58}Ni,$2pn$) and ^{58}Ni(^{64}Zn,$2pn$) reactions have been used, for which the predicted cross sections are several mb. High-spin spectroscopy was performed using the GAMMASPHERE array, and isotopic and isobaric identifications were made in a separate experiment using the Argonne Fragment Mass Analyzer (FMA) [25] where gamma-recoil and gamma–x-ray coincidences were observed, confirming the assignment of these bands to ^{119}Ba.

II. EXPERIMENTAL DETAILS

A. GAMMASPHERE experiment: High-spin spectroscopy

Details of the experiments have already been given in Refs. [1,23,26]. In the first experiment, high-spin states were populated using the ^{58}Ni(^{64}Zn,$2pn$)^{119}Ba reaction and deexcitation gamma rays were detected using the GAMMASPHERE array. The 265-MeV ^{64}Zn beam was accelerated by the 88-Inch Cyclotron at the Lawrence Berkeley National Laboratory. The beam was incident upon two stacked 500-μg/cm^2, self-supporting, 99%-pure ^{58}Ni foils. At the time of the experiment, GAMMASPHERE had 56, 75%-efficient escape-suppressed germanium detectors in place. The detectors were arranged in 14 rings with constant polar angle θ: two detectors at $\theta=17.3°$, five at 31.7°, five at 37.4°, five at 50.1°, one at 58.3°, one at 80.7°, six at 90.0°, one at 99.3°, one at 100.8°, five at 121.7°, ten at 129.9°, five at 142.6°, four at 148.3°, and five at 162.7°. With the requirement that at least three germanium detectors fired in prompt coincidence before data were recorded, a total of 9×10^8 gamma-ray coincidence events were written to magnetic tape. In the off-line analysis each n-fold event ($n\geqslant3$) was decomposed into $^nC_3$ threefold gamma-ray coincidences, yielding a total of 6×10^9 unfolded triples which were subsequently used to increment a three-dimensional histogram (cube). The RADWARE software package [27] was used to analyze the data. By gating on known transitions, approximately 15 nuclei were observed. The most intensely populated nuclei were ^{119}Cs ($3p$ evaporation), ^{118}Xe ($4p$), and ^{116}Xe ($\alpha2p$) which were produced with approximately 33%, 30%, and 19% of the evaporation-residue cross section, respectively. From the GAMMASPHERE data, two bands were tentatively assigned to ^{119}Ba purely on the basis of excitation-energy systematics and the lack of coincidences with gamma rays in any known nuclei. These bands were populated with about 2% of the total evaporation-residue cross section, corresponding to about 5 mb. Figure 1 shows representative spectra projected from the cube by applying gates to two of the three axes.

B. ATLAS/FMA experiment: Assignment of excited states to ^{119}Ba

In order to confirm that the two bands observed with GAMMASPHERE belonged to ^{119}Ba, a second experiment was performed in which gamma rays were detected in coincidence with recoiling evaporation residues and with x rays. In this experiment the ^{64}Zn(^{58}Ni,$2pn$)^{119}Ba reaction was used.

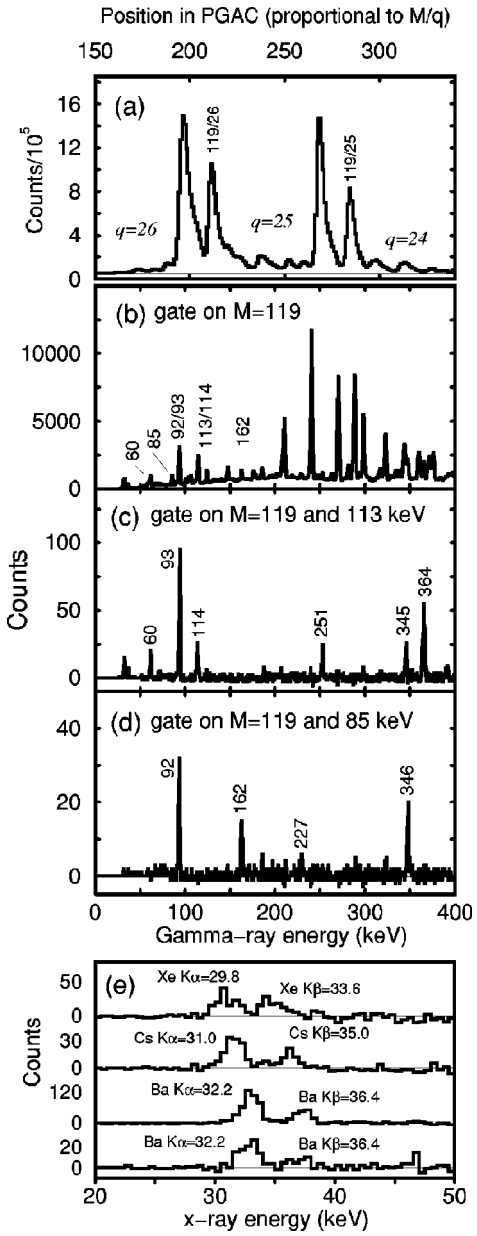

FIG. 2. Results from the ATLAS/FMA experiment. Panel (a) shows the spectrum of recoils recorded at the focal plane of the FMA. The peaks corresponding to $A=119$ recoils are labeled with M/q. Panel (b) shows the total projection of a $\gamma\gamma$ matrix gated on $M=119$ recoils; the most intense peaks in the spectrum belong to ^{119}Cs. Several of the ^{119}Ba peaks are labeled with transition energies. Panel (c) shows a spectrum projected from the $M=119$ gated matrix, gated on the 113-keV transition. Panel (d) shows a spectrum which is also projected from the $M=119$ gated matrix, gated on the 85-keV transition. Panel (e) shows the K x-ray regions of spectra projected from a matrix which was not gated by mass. The lower-middle and lower spectra are gated on the 113- and 161-keV transitions, respectively. The upper and upper-middle spectra show K x rays in coincidence with uncontaminated gamma-ray gates on ^{118}Xe and ^{119}Cs, respectively. In panel (c), the 113-keV gate will overlap with the 114-keV transition, which explains the coincidence with the 364-keV transition.

The ^{58}Ni beam, at energies of 230 and 240 MeV, was provided by the Argonne Tandem Linac Accelerator System (ATLAS). The target was a self-supporting ^{64}Zn foil of thickness 500 μg/cm^2. Gamma rays and x rays were detected at the reaction site in an array of ten Compton-suppressed 25%-efficient germanium detectors; the thresholds on two of the detectors were reduced in order to detect $\sim$35-keV barium K x rays. The recoiling reaction products were dispersed according to their mass-to-charge state ratio and detected in a parallel-grid avalanche counter (PGAC) at the focal plane of the FMA. With the trigger condition of two or more Ge detector signals in coincidence with each other, or one or more Ge signals in coincidence with a PGAC signal, approximately 9×10^7 events were recorded.

The spectrum recorded by the PGAC is shown in Fig. 2(a). Mass-119 recoils with two different charge states were detected by the PGAC, but the majority of these were ^{119}Cs residues. The data were sorted into gamma-gamma correlation matrices gated on recoils with masses 115–120 and an ungated (no recoil condition) matrix. The method used to assign excited states to ^{119}Ba is the same as that described for ^{118}Ba and ^{118}Cs in Refs. [1,26]. Figure 2(b) shows the total projection of the $M=119$ gated matrix. Some of the transitions belonging to ^{119}Ba are labeled with their transition energies. Figure 2(c) shows gamma rays in coincidence with an $M=119$ recoil and a 113-keV gamma ray. Similarly, Fig. 2(d) shows gamma rays in coincidence with an $M=119$ recoil and an 85-keV gamma ray. Figures 2(c) and 2(d) show the same coincident transitions as would be expected from the GAMMASPHERE data and confirm that the bands belong to a nucleus with mass 119. Figure 2(e) shows the K x ray region of several spectra projected from the ungated matrix. The lower-middle and lower spectra of Fig. 2(e) are gated on the 113-keV and 161-keV transitions, respectively. The upper and upper-middle spectra are gated on ^{118}Xe (472-keV) and ^{119}Cs (269-keV) transitions, respectively. The K x rays in coincidence with the suspected ^{119}Ba bands are clearly barium K x rays, confirming the assignment of the bands to ^{119}Ba.

III. RESULTS: LEVEL SCHEME OF ^{119}Ba

Coincidence relationships, together with energy- and intensity-balance arguments, have been used to deduce the level structures presented in Fig. 3. Two independent rotational bands, labeled Band 1 and Band 2, have been observed. No transitions have been observed linking the two bands, so their relative spins and excitation energies have not been established. Excitation-energy systematics in the odd-A barium isotopes and aligned angular momentum arguments (which are discussed in Sec. IV) suggest that Band 1 is based on the $\nu(h_{11/2})[532]5/2^-$ orbital and Band 2 is based on the $\nu(g_{7/2}d_{5/2})[413]5/2^+$ orbital. The spin and parity assignments of the bandheads are taken from systematics and are therefore tentative. The energies and relative intensities of all of the transitions assigned to ^{119}Ba are given in Table I.

In order to help assign relative spin and parity values to the excited states, a type of gamma-ray angular distribution measurement was used. Two gamma-gamma correlation ma-

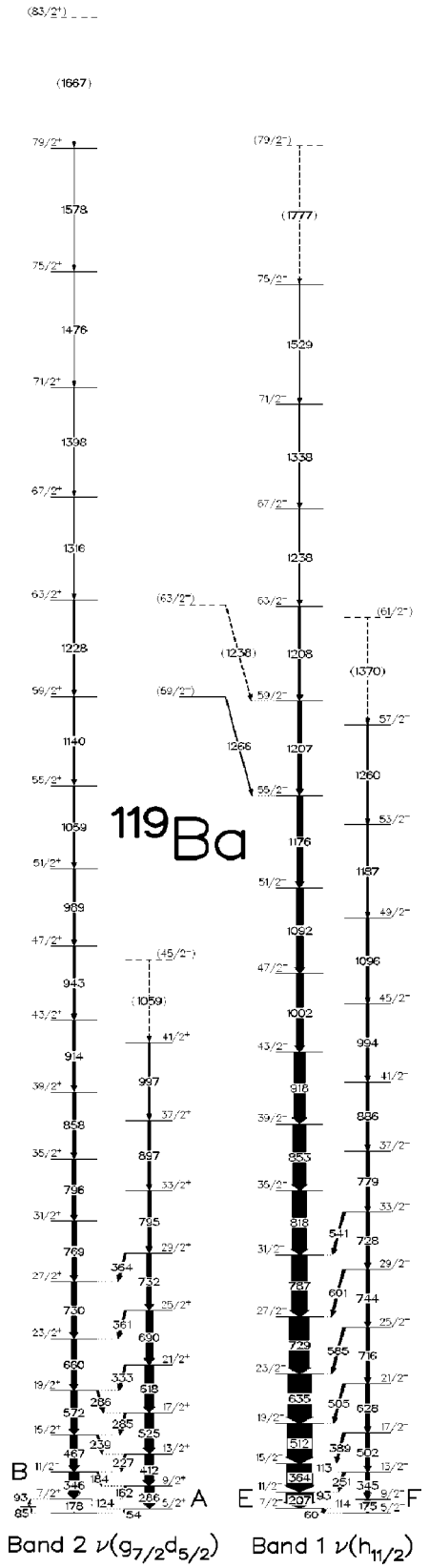

FIG. 3. The level structure of ^{119}Ba deduced in this work. The uncertainties in the intensities range from ~5 to 20% and those in the energies are all less than 0.3 keV. The spins of all of the levels are taken from systematics and are therefore tentative.

trices were constructed, which were incremented with gamma-ray energies from any germanium detector, independent of angle, on one axis, and with gamma-ray energies from detectors at a particular value of θ (and $180-\theta$) on the other axis. By gating on the any-germanium-detector axis, the intensities of gamma rays detected at θ could be measured in the resulting spectrum. Using this method, the intensities of the gamma rays in the detectors with $\theta \simeq 90°$ (6 detectors), and $\theta \simeq (50$ or $130)°$ (34 detectors) were measured, and the ratio (R_{ang}) of these intensities was taken. After normalization, the ratio was found to be near 0.7 for a stretched-dipole transition and near 1.3 for a stretched-quadrupole transition. The values were calibrated using known transitions in the well-studied ^{119}Cs [28] and ^{118}Xe [23,29] nuclei. Using this method, the relative spin assignments up to $(47/2)\hbar$ in Band 1 and $(29/2)\hbar$ in Band 2 were made. The values of the measured angular intensity ratios (R_{ang}) are given in Table I, together with the probable multipolarities of the gamma rays.

Assuming that the spin assignments are correct, Band 1 and Band 2 extend to $(75/2)\hbar$ [tentatively $(79/2)\hbar$] and $(79/2)\hbar$ [tentatively $(83/2)\hbar$], respectively. These spins are approximately $6\hbar$ above any known spins in other odd-A barium isotopes. Both bands consist of two $\Delta I=2$ signature-partner sequences connected by $\Delta I=1$ transitions below $(31/2)\hbar$. Henceforth, the standard convention shall be adopted (see Sec. IV and, for example, Ref. [30]), and the signature partner sequences will be referenced by the letters A, B, E, and F, as indicated in Fig. 3. Band 1F is observed up to $(57/2)\hbar$ [tentatively $(61/2)\hbar$] while Band 1E is observed up to $(75/2)\hbar$ [tentatively $(79/2)\hbar$]. Transitions with $\Delta I=1$, presumed to be of $M1/E2$ character, are observed in Band 1 below $(33/2)\hbar$. The signature splitting is about 180 keV at a rotational frequency of about 0.3 MeV/$\hbar$, as would be expected for a band built on the $[532]5/2^-$ orbital. Similarly, Band 2A is observed up to spin $(41/2)\hbar$ [tentatively $(45/2)\hbar$] while Band 2B is observed up to $(79/2)\hbar$ [tentatively $(83/2)\hbar$]. In Band 2, $\Delta I=1 M1/E2$ transitions are observed connecting the signature partners below $(29/2)\hbar$. The signature splitting is almost zero (before the first quasiparticle alignment) consistent with the $\nu(g_{7/2}d_{5/2})[413]5/2^+$ assignment.

In addition to the in-band transitions, four low-energy, low-intensity transitions are observed below Band 2; the transitions have energies of 54, 85, 93, and 178 keV. Coincidence relationships between these transitions and the lower members of Band 2 are shown in the spectra of Fig. 4, panels (a), (b), and (c), while an expanded part of the level scheme is shown in Fig. 4, panel (d). It is presumed that the four transitions are not a continuation of Band 2 because of their very low intensity relative to the lowest members of the band. It is possible that the $7/2^+$ state is isomeric, although it is not possible to investigate this further with the present data set.

IV. DISCUSSION

A. Excitation-energy systematics

In the odd-A, $A \simeq 120$ barium isotopes, the energies of the lowest-lying states, relative to the bandhead, in the $\nu(h_{11/2})$

TABLE I. Properties of the transitions assigned to ^{119}Ba, from the GAMMASPHERE data.

E_γ [a]	I [b]	R_{ang}	$I_i^{\pi_i} \rightarrow I_f^{\pi_f}$	$\sigma\lambda$	E_γ [a]	I [b]	R_{ang}	$I_i^{\pi_i} \rightarrow I_f^{\pi_f}$	$\sigma\lambda$
54.3	0.9(5)		$\frac{5}{2}^+ \rightarrow (\frac{3}{2}^+)$ [g]		729.8	35(7)		$\frac{27}{2}^+ \rightarrow \frac{23}{2}^+$	$E2$
60.1	~ 2 [c]	0.69(10)	$\frac{7}{2}^- \rightarrow \frac{5}{2}^-$	$M1/E2$	731.6	53(10)		$\frac{29}{2}^+ \rightarrow \frac{25}{2}^+$	$E2$
85.1	0.6(4)	0.29(11)	$\frac{5}{2}^+ \rightarrow (\frac{3}{2}^+)$ [g]		744.4	17.2(0.9)	1.37(14)	$\frac{29}{2}^- \rightarrow \frac{25}{2}^-$	$E2$
92.6	0.7(4)	0.75(24)	$\frac{7}{2}^+ \rightarrow \frac{5}{2}^+$		768.5	33.9(0.7)		$\frac{31}{2}^+ \rightarrow \frac{27}{2}^+$	$E2$
92.8	3.0(7)	0.68(8)	$\frac{11}{2}^- \rightarrow \frac{9}{2}^-$	$M1/E2$	779.1	11(4)	1.07(12)	$\frac{37}{2}^- \rightarrow \frac{33}{2}^-$	$E2$
112.6	2.0(6) [d]	0.72(7) [d]	$\frac{15}{2}^- \rightarrow \frac{13}{2}^-$	$M1/E2$	787.2	70.9(1.4)	1.15(11)	$\frac{31}{2}^- \rightarrow \frac{27}{2}^-$	$E2$
113.6	2.0(6) [d]	0.72(7) [d]	$\frac{9}{2}^- \rightarrow \frac{7}{2}^-$	$M1/E2$	794.8	50(10)		$\frac{33}{2}^+ \rightarrow \frac{29}{2}^+$	$E2$
123.5	0.9(2)	0.58(15)	$\frac{7}{2}^+ \rightarrow \frac{5}{2}^+$	$M1/E2$	796.2	26.8(1.3)		$\frac{35}{2}^+ \rightarrow \frac{31}{2}^+$	$E2$
161.9	48.5(5.0)	0.72(11)	$\frac{9}{2}^+ \rightarrow \frac{7}{2}^+$	$M1/E2$	817.9	58.1(2.9)	1.36(12)	$\frac{35}{2}^- \rightarrow \frac{31}{2}^-$	$E2$
174.9	30(10) [h]	1.23(21)	$\frac{9}{2}^- \rightarrow \frac{5}{2}^-$	$E2$	852.7	39.0(2.0)	1.47(16)	$\frac{39}{2}^- \rightarrow \frac{35}{2}^-$	$E2$
177.6	0.4(1)	0.83(22)	$\frac{7}{2}^+ \rightarrow (\frac{3}{2}^+)$ [g]	$E2$	858.4	24(6)		$\frac{39}{2}^+ \rightarrow \frac{35}{2}^+$	$E2$
184.0	13.9(2.0)	0.85(10)	$\frac{11}{2}^+ \rightarrow \frac{9}{2}^+$	$M1/E2$	885.5	9.8(0.5)	1.56(18)	$\frac{41}{2}^- \rightarrow \frac{37}{2}^-$	$E2$
207.0	115(15) [h]	1.05(1)	$\frac{11}{2}^- \rightarrow \frac{7}{2}^-$	$E2$	896.8	51(10)		$\frac{37}{2}^+ \rightarrow \frac{33}{2}^+$	$E2$
227.5	29.5(1.5)	0.53(8)	$\frac{13}{2}^+ \rightarrow \frac{11}{2}^+$	$M1/E2$	913.8	28.0(1.4)		$\frac{43}{2}^+ \rightarrow \frac{39}{2}^+$	$E2$
239.0	9.7(5)	0.59(10)	$\frac{15}{2}^+ \rightarrow \frac{13}{2}^+$	$M1/E2$	917.8	44.1(2.2)	1.28(14)	$\frac{43}{2}^- \rightarrow \frac{39}{2}^-$	$E2$
250.9	7.7(4)	0.72(10)	$\frac{13}{2}^- \rightarrow \frac{11}{2}^-$	$M1/E2$	942.6	13.4(0.7)		$\frac{47}{2}^+ \rightarrow \frac{43}{2}^+$	$E2$
285[e]	10(5)		$\frac{17}{2}^+ \rightarrow \frac{15}{2}^+$	$M1/E2$	988.6	16.5(0.8)		$\frac{51}{2}^+ \rightarrow \frac{47}{2}^+$	$E2$
286[e]	73(10) [h]	0.59(14) [d]	$\frac{9}{2}^+ \rightarrow \frac{5}{2}^+$	$E2$	994.3	9.5(0.5)	1.37(18)	$\frac{45}{2}^- \rightarrow \frac{41}{2}^-$	$E2$
286.2	4(1)		$\frac{19}{2}^+ \rightarrow \frac{17}{2}^+$	$M1/E2$	996.6	28(7)		$\frac{41}{2}^+ \rightarrow \frac{37}{2}^+$	$E2$
332.8	~ 5 [c]	0.81(15)	$\frac{21}{2}^+ \rightarrow \frac{19}{2}^+$	$M1/E2$	1002.1	32.5(1.6)	1.50(21)	$\frac{47}{2}^- \rightarrow \frac{43}{2}^-$	$E2$
344.7	25(5)		$\frac{13}{2}^- \rightarrow \frac{9}{2}^-$	$E2$	1059.3	11(4)		$(\frac{45}{2}^+) \rightarrow \frac{41}{2}^+$	$E2$
346.3	55(6)	1.38(15)	$\frac{11}{2}^+ \rightarrow \frac{7}{2}^+$	$E2$	1059.5	19.3(1.0)		$\frac{55}{2}^+ \rightarrow \frac{51}{2}^+$	$E2$
361.1	~ 5 [c]		$\frac{25}{2}^+ \rightarrow \frac{23}{2}^+$	$M1/E2$	1092.3	30.7(1.5)		$\frac{51}{2}^- \rightarrow \frac{47}{2}^-$	$E2$
363.7	110(15) [h]	1.15(12)	$\frac{15}{2}^- \rightarrow \frac{11}{2}^-$	$E2$	1096.1	6.9(1.4)		$\frac{49}{2}^- \rightarrow \frac{45}{2}^-$	$E2$
363.8	~ 2 [c]		$\frac{29}{2}^+ \rightarrow \frac{27}{2}^+$	$M1/E2$	1139.9	12.9(2.6)		$\frac{59}{2}^+ \rightarrow \frac{55}{2}^+$	$E2$
389.1	3.5(0.2)	0.55(5)	$\frac{17}{2}^- \rightarrow \frac{15}{2}^-$	$M1/E2$	1176.3	25.4(3.8)		$\frac{55}{2}^- \rightarrow \frac{51}{2}^-$	$E2$
411.9	65(10) [h]	1.17(13)	$\frac{13}{2}^+ \rightarrow \frac{9}{2}^+$	$E2$	1187.3	6.5(3)		$\frac{53}{2}^- \rightarrow \frac{49}{2}^-$	$E2$
467.1	49.2(2.5)	0.95(18)	$\frac{15}{2}^+ \rightarrow \frac{11}{2}^+$	$E2$	1207[e]	10(4)		$\frac{59}{2}^- \rightarrow \frac{55}{2}^-$	$E2$
502.4	30(5) [h]		$\frac{17}{2}^- \rightarrow \frac{13}{2}^-$	$E2$	1208.2	10(3)		$\frac{63}{2}^- \rightarrow \frac{59}{2}^-$	$E2$
505.3	1.5(0.4)	0.48(5)	$\frac{21}{2}^- \rightarrow \frac{19}{2}^-$	$M1/E2$	1228.5	7.8(1.6)		$\frac{63}{2}^+ \rightarrow \frac{59}{2}^+$	$E2$
512.5	105(10) [h]	1.20(10)	$\frac{19}{2}^- \rightarrow \frac{15}{2}^-$	$E2$	1237.5	8.7(1.7)		$\frac{67}{2}^- \rightarrow \frac{63}{2}^-$	$E2$
524.6	60(6) [h]	1.22(14)	$\frac{17}{2}^+ \rightarrow \frac{13}{2}^+$	$E2$	1238[e]	~ 1 [c]		$(\frac{63}{2}^-) \rightarrow \frac{59}{2}^-$	$E2$
541.3	~ 1 [c]	0.46(9)	$\frac{33}{2}^- \rightarrow \frac{31}{2}^-$	$M1/E2$	1259.7	7.6(1.5)		$\frac{57}{2}^- \rightarrow \frac{53}{2}^-$	$E2$
571.7	45.3(2.3)	1.06(16)	$\frac{19}{2}^+ \rightarrow \frac{15}{2}^+$	$E2$	1266.3	~ 10 [c]		$(\frac{59}{2}^-) \rightarrow \frac{55}{2}^-$	$E2$
585.2	~ 1 [c]	0.67(13)	$\frac{25}{2}^- \rightarrow \frac{23}{2}^-$	$M1/E2$	1316.2	9.5(1.9)		$\frac{67}{2}^+ \rightarrow \frac{63}{2}^+$	$E2$
601.3	~ 1 [c]	0.50(10)	$\frac{29}{2}^- \rightarrow \frac{27}{2}^-$	$M1/E2$	1337.5	9.6(1.9)		$\frac{71}{2}^- \rightarrow \frac{67}{2}^-$	$E2$
618.3	57(10) [d]	1.19(15)	$\frac{21}{2}^+ \rightarrow \frac{17}{2}^+$	$E2$	1370.1	1.9(0.4)		$(\frac{61}{2}^-) \rightarrow \frac{57}{2}^-$	$E2$
627.9	27(5) [h]	1.08(10)	$\frac{21}{2}^- \rightarrow \frac{17}{2}^-$	$E2$	1397.6	8.7(1.7)		$\frac{71}{2}^+ \rightarrow \frac{67}{2}^+$	$E2$
635.4	100.0(5.0)	1.25(11)	$\frac{23}{2}^- \rightarrow \frac{19}{2}^-$	$E2$	1475.7	4.5(0.9)		$\frac{75}{2}^+ \rightarrow \frac{71}{2}^+$	$E2$
659.6	38.0(1.9)		$\frac{23}{2}^+ \rightarrow \frac{19}{2}^+$	$E2$	1529.2	6.3(1.3)		$\frac{75}{2}^- \rightarrow \frac{71}{2}^-$	$E2$
689.5	55(10) [d]	1.01(14)	$\frac{25}{2}^+ \rightarrow \frac{21}{2}^+$	$E2$	1578.0	2.1(0.5)		$\frac{79}{2}^+ \rightarrow \frac{75}{2}^+$	$E2$
716.4	25.9(1.3)	1.43(16)	$\frac{25}{2}^- \rightarrow \frac{21}{2}^-$	$E2$	1666.8	1.2(0.3)		$\frac{83}{2}^+ \rightarrow \frac{79}{2}^+$	$E2$
727.9	14(4) [d]	0.94(20)	$\frac{33}{2}^- \rightarrow \frac{29}{2}^-$	$E2$	1776.8	1.9(0.5)		$\frac{79}{2}^- \rightarrow \frac{75}{2}^-$	$E2$
728.7	90(10) [h]	1.33(12)	$\frac{27}{2}^- \rightarrow \frac{23}{2}^-$	$E2$					

[a] Energies typically accurate to 0.2 or 0.3 keV.

[b] Intensities relative to the 627.9-keV transition. Uncertainties in the intensities include a 5% contribution from the efficiency calibration.

[c] Intensity estimated, not measured.

[d] Result for composite peak.

[e] Energy estimated, not measured.

[g] Most likely spins of states (in parentheses).

[h] Uncertainty in intensity includes contribution from normalization of gating transitions.

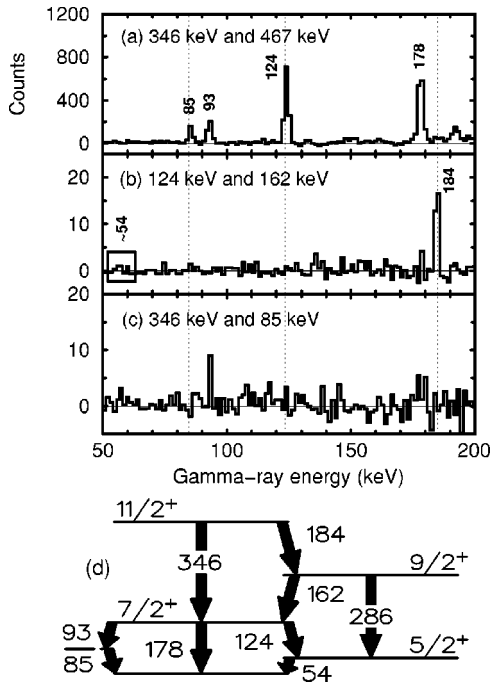

FIG. 4. (a), (b), and (c) are coincidence spectra showing the transitions below Band 2. The spectra are gated on the transitions given on the figure (top left of each panel). Panel (d) is an enlarged portion of the level scheme, showing the low-spin levels in Band 2.

and $\nu(g_{7/2}d_{5/2})$ bands vary smoothly as a function of neutron number. The systematics are shown in Fig. 5; part (a) shows the negative-parity bands in the odd-A, $A<130$ barium isotopes, for spins up to $(27/2)\hbar$, and part (b) shows the positive-parity bands, for spins up to $(23/2)\hbar$. Taking the spin assignments of Fig. 3, the bands observed in this work fit these trends well. The signature splitting is clearly larger in the negative-parity bands than in the positive-parity bands, as would be expected for the $\nu(h_{11/2})[532]5/2^-$ and $\nu(g_{7/2}d_{5/2})[413]5/2^+$ assignments. For the negative-parity bands, the energy difference between the $11/2^-$ state and the $15/2^-$ state decreases continuously from $A=129$ down to $A=119$, which suggests an increase in deformation. This is consistent with theory [31]; the theory of Ref. [31] predicts that the deformation should peak between $A=117$ and $A=121$, which agrees with the smaller change in this energy difference for the lowest masses.

As pointed out in Ref. [3], a comparison of the positive-parity level energies should be treated cautiously, since it has been shown by measurement of the magnetic moments that the $5/2^+$ states in ^{121}Ba and ^{123}Ba, for example, have different origins. In ^{121}Ba, the spin and parity of the ground state have been measured to be $5/2^+$ [32], and a positive magnetic moment suggests that the ground state is the $\nu(d_{5/2})[413]5/2^+$ orbital. However, in ^{123}Ba, a measured negative magnetic moment suggests that the ground state is the $\nu(g_{7/2})[402]5/2^+$ orbital. In ^{121}Ba the band shown in Fig. 5(b) is built directly on the $5/2^+$ ground state. In ^{119}Ba, no measurement of the ground-state spin and parity has been made. However, a comparison of β-delayed proton-emission spectra with a statistical model in Ref. [33] has suggested that the ground state has $I^\pi=5/2^+$. In the present work, four transitions are observed below Band 2, which do not appear to be a continuation of the band. This observation suggests that either there are structural changes in the positive-parity rotational spectrum of ^{119}Ba, which mean that the excitation-energy systematics are not reliable or that the ground state of ^{119}Ba does not have $I^\pi=5/2^+$.

B. Quasiparticle alignments

The configurations underlying rotational bands can be investigated by studying their aligned angular momenta. In high-spin bands such as those presented in Fig. 3, the aligned angular momenta can easily be extracted according to the standard prescription described in Ref. [34]. The aligned angular momenta (i_x) for the bands in ^{119}Ba are presented as a function of rotational frequency in Fig. 6; for all data points, a reference angular momentum has been subtracted, with the Harris parameters [35] $\mathcal{J}_0=17.0$ MeV$^{-1}\hbar^2$ and $\mathcal{J}_1=25.8$ MeV$^{-3}\hbar^4$. By comparing the experimental alignments with those predicted theoretically, and by applying Pauli blocking arguments, information about the underlying configurations can be obtained. In this work, a standard procedure has been adopted, whereby total Routhian surface (TRS) [36,37] calculations are used to estimate the deformations of the suspected configurations, and these deformations are subsequently used as input into Woods-Saxon cranked shell model (CSM) calculations [38,39] in order to extract theoretical quasiparticle alignment frequencies. These calculated alignment frequencies can then be compared to those observed experimentally.

The TRS calculations predict axially symmetric prolate shapes for both bands in ^{119}Ba, at low and intermediate spins. At a representative rotational frequency of $\hbar\omega=0.183$ MeV, the $\nu(h_{11/2})$ configuration is predicted to have deformation parameters of $\beta_2\simeq0.27$, $\beta_4\simeq0.03$, and $\gamma\simeq-4°$. At the same frequency, the $\nu(g_{7/2}d_{5/2})$ configuration is predicted to have $\beta_2\simeq0.28$, $\beta_4\simeq0.04$, and $\gamma\simeq0°$. Using these deformation parameters, Woods-Saxon cranked shell model calculations predict the alignment of the pairs of neutrons and protons from the $h_{11/2}$ subshell in the observed rotational frequency range. [Alignments of pairs of neutrons and protons from the $(g_{7/2}d_{5/2})$ subshell are not expected to occur below 0.7 MeV/$\hbar$.] The predicted alignment frequencies are given in Table II.

If Band 1 has a $\nu(h_{11/2})$ configuration, then the first $h_{11/2}$ neutron (EF) alignment will be blocked, for both signatures. However, the first alignment of $h_{11/2}$ protons (ef) and of subsequent pairs of $h_{11/2}$ neutrons (the FG alignment in the favored E configuration and EH in the unfavored F configuration) are possible sources of additional alignment. Figure 6(a) reveals a gain in i_x for both signatures of Band 1 at about 0.36 MeV/$\hbar$, which is attributed to the ef proton alignment. (The slight difference in alignment frequencies for each of the two signatures can be ascribed to subtle differences in deformation.) The subsequent $h_{11/2}$ neutron alignments, FG and EH, are predicted to occur at 0.53 and 0.58 MeV/$\hbar$, respectively, in this band, but there are no obvious gains in i_x at these frequencies. There are several

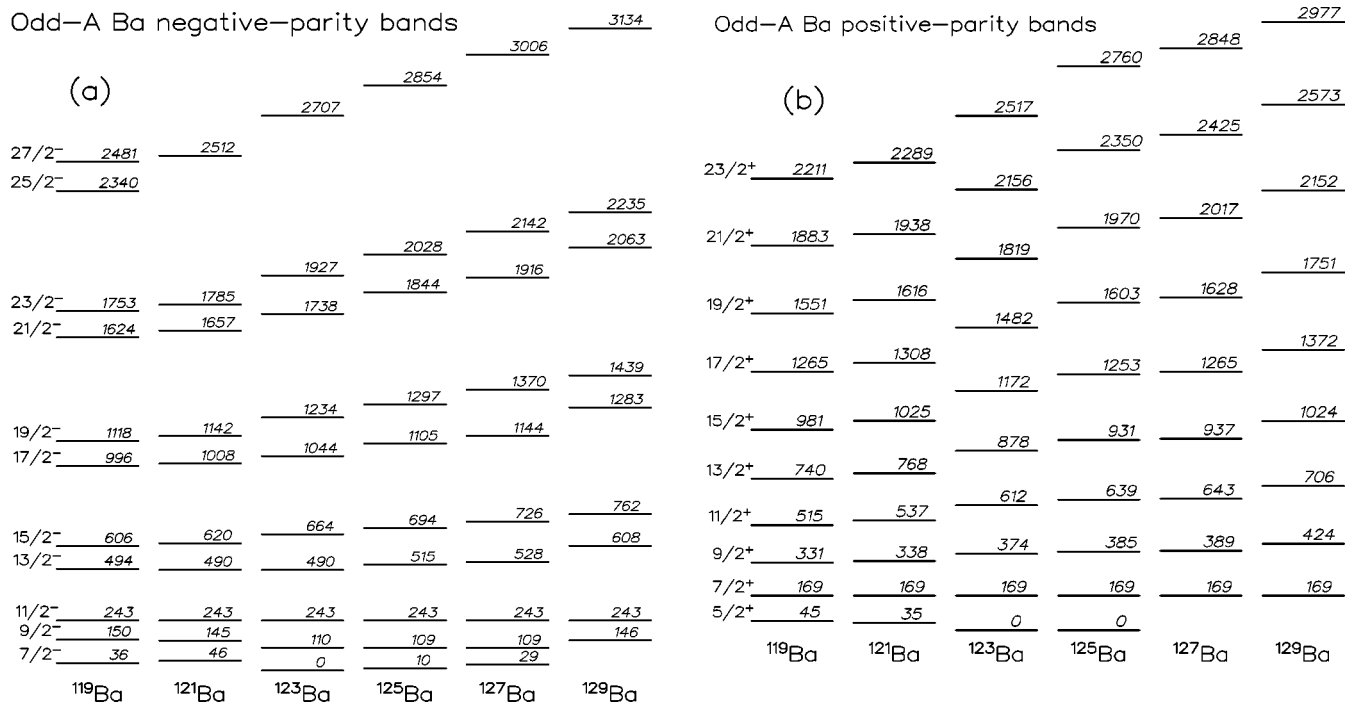

FIG. 5. Excitation-energy systematics for bands in odd-A ($A<130$) barium isotopes. (a) shows negative-parity bands; the energies are shown relative to the position of the $11/2^-$ state in each band. (b) shows positive-parity bands; the energies are shown relative to the position of the $7/2^+$ states. The data for $^{121-129}$Ba are taken from Refs. [3–8].

possible explanations for this nonobservation. First of all it is possible that the alignment does indeed take place at the predicted frequency, but that the interaction strength is very large, so that no upbend is apparent. However, this is unlikely because, above the first (ef) alignment, the i_x curve is essentially flat, especially in Band 1F. A second possibility is that both the FG and EH alignments are delayed significantly, and the upbend in i_x at 0.60 MeV/$\hbar$ in Band 1E is due to the FG alignment, with the expected EH alignment in Band 1F being delayed to a higher frequency than that experimentally observed. However, it is also likely that the upbend at 0.60 MeV/$\hbar$ in Band 1E is caused by the perturbation of the in-band level energies by the two sidefeeding states shown in Fig. 3. A third possibility is that the nucleons in ^{119}Ba are aligning in a more continuous manner, as will be discussed in Sec. IV D.

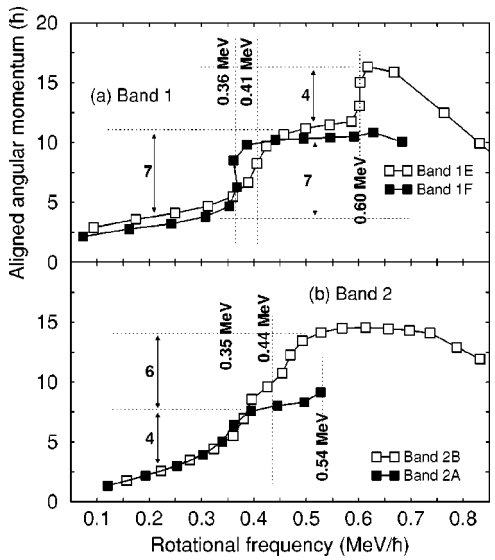

FIG. 6. Experimentally extracted aligned angular momenta for ^{119}Ba, plotted as a function of rotational frequency. A reference configuration has been subtracted with the Harris parameters [35] $\mathcal{J}_0=17.0$ MeV$^{-1}\hbar^2$ and $\mathcal{J}_1=25.8$ MeV$^{-3}\hbar^4$. Panel (a) shows the data for Band 1 and panel (b) shows the data for Band 2. The numbers in bold, near the vertical arrows, give the alignment gains, in units of $\hbar$.

Band 2 is presumed to have a $\nu(g_{7/2}d_{5/2})$ configuration. If this is correct, then neither the first $h_{11/2}$ proton (ef) nor neutron (EF) alignments are blocked and both should be experimentally observed. Initially both signatures of Band 2 behave in a similar manner, and both exhibit an alignment at 0.35 MeV/$\hbar$. Like in Band 1, this first alignment is attributed to the first pair of $h_{11/2}$ protons (ef). Following this alignment, the signature splitting between the two bands increases. In Band 2B, a second alignment is observed at about 0.44 MeV/$\hbar$ which is probably due to the first pair of $h_{11/2}$ neutrons (EF). In Band 2A, no second alignment is observed at least until 0.54 MeV/$\hbar$.

C. Moments of inertia

It can be seen in Fig. 3 that at the highest spins in Band 1, the gamma rays have rather large energy and the spacing between levels appears to be greater than what might be expected for a rotational band. The dynamic ($\mathcal{J}^{(2)}$) moments of inertia are calculated as $\mathcal{J}^{(2)}=4/\Delta E_\gamma$, and hence reveal this large level spacing. The dynamic moments of inertia for

TABLE II. Predicted alignment frequencies at the deformations calculated for the bands in ^{119}Ba. The labels ef (EF), fg (FG), eh (EH), and ab (AB) refer to the specific pairs of $h_{11/2}$ protons (neutrons) and the $(g_{7/2}d_{5/2})$ protons (neutrons), respectively. This nomenclature is detailed in, for example, Ref. [30]. The deformations used in the calculations are given in the text. Columns (a) and (b) give the predicted alignment frequencies in bands 1 and 2, respectively, although for the given configurations of the bands, several of the alignments will be Pauli blocked.

	Alignment frequency (MeV/$\hbar$)	
Aligning nucleons	(a) Band 1 [$\nu(h_{11/2})$]	(b) Band 2 [$\nu(g_{7/2}d_{5/2})$]
π(ef)	0.36	0.38
π(fg)	0.54	0.54
π(eh)	0.56	0.57
π(ab)	>0.7	>0.7
ν(EF)	0.36	0.40
ν(FG)	0.53	0.52
ν(EH)	0.58	0.56
ν(AB)	>0.7	>0.7

Bands 1 and 2 are plotted in Fig. 7. Above about 0.6 MeV/$\hbar$, the observed $\mathcal{J}^{(2)}$ for Band 1 clearly shows a decreasing trend with increasing frequency. This feature is characteristic of smooth terminating bands in lighter nuclei in the region just above $Z=50$, which are based on two-particle–two-hole excitations across the $Z=50$ gap. In Band 2, however, the spacings between the transition energies do not change as rapidly as Band 1, as a function of rotational frequency, leading to a constant $\mathcal{J}^{(2)}$ moment of inertia.

D. Smooth band termination

In order to achieve a microscopic understanding of the high-spin bands in ^{119}Ba, calculations have been carried out within the framework of the configuration-dependent cranked Nilsson-Strutinsky approach [12,40] with the same parameters as in these references. A plot of the energies of states in the bands of ^{119}Ba, minus a rigid-rotor reference, is shown in Fig. 8 in comparison with the theoretical configurations. The curves are only shown above $20\hbar$ because pairing is not included in the calculations; comparisons are therefore not meaningful at low spins. The calculated configurations are labeled using the shorthand notation $[p,n]$, where p represents the number of $h_{11/2}$ protons and n represents the number of $h_{11/2}$ neutrons involved in the configuration (though it should be pointed out that this labeling scheme is only relevant at high spin). In the figure, the superscripts attached to the configuration labels give the sign of the total signature quantum number α. These bands are interpreted as being built in the valence space involving orbitals from the subshells above the $Z=50$ and $N=50$ gaps. The earlier discussion of excitation-energy systematics and quasiparticle alignments suggests that Bands 1E and 2B will have the $[2,3]^-$ and $[2,4]^-$ configurations, respectively, at high spin. With the spin assignments taken from systematics, the calculations for the $[2,3]^-$ and $[2,4]^-$ configurations are in good agreement with the experimental data for Band 1E and Band 2B, respectively. Specifically the slopes of the experimental data points are reproduced well by the calculations. Since the calculations do not include pairing, the excitation energies are only relative [the excitation energies of both bandheads have been set to zero in Fig. 8(b)].

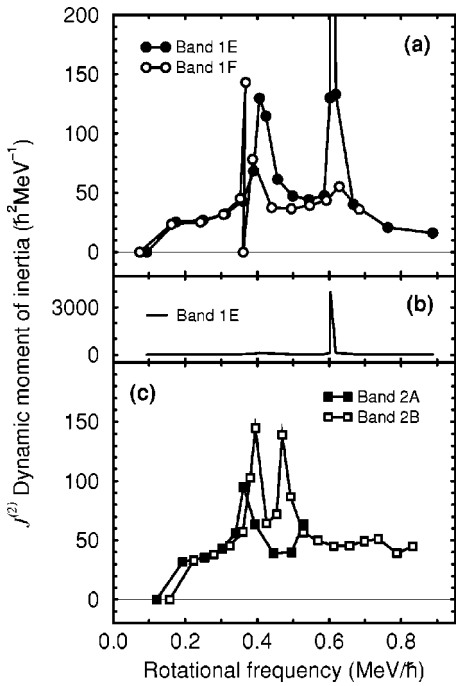

FIG. 7. Experimentally extracted dynamic ($\mathcal{J}^{(2)}$) moments of inertia for ^{119}Ba. Panels (a) and (b) show data for band 1: panel (a) shows the low $\mathcal{J}^{(2)}$ section in detail, while panel (b) shows all the data points. Panel (c) shows the data for band 2.

For the $[2,3]^-$ configuration, the calculations predict several aligned states, of which three are shown on Fig. 8(a). The first of these is found at $I^\pi=83/2^-$ and is based upon the $\nu[(g_{7/2}d_{5/2})^{10}(h_{11/2})^3]_{43/2^-}\otimes\pi[(g_{7/2}d_{5/2})^4(h_{11/2})^2]_{20^+}$ configuration. In this specific state the ten $(g_{7/2}d_{5/2})$ neutrons couple to $I=8\hbar$ rather than the maximal value of $I=10\hbar$. The maximum spin state which can be formed with all ten $N=4$ low-j neutrons in $(g_{7/2}d_{5/2})$ orbitals is $87/2^-$ but this state is not calculated to be yrast. Instead, the yrast states for this configuration are formed with one or two neutrons excited to the $(d_{3/2}s_{1/2})$ orbitals, resulting in the aligned state at $I^\pi=91/2^-$ and the final terminating state at $I^\pi=95/2^-$. The high energy cost of generating spin above the first aligned state is clearly seen in Fig. 8(a), where, relative to the reference, the final terminating state at $(95/2)\hbar$ lies more than 2 MeV above the state at $(83/2)\hbar$. For the $[2,4]^-$ configuration, the calculations predict two aligned states, at $I^\pi=91/2^+$ and $99/2^+$. Like in the $[2,3]^-$ configuration, the lowest-lying aligned state is formed by coupling the $(g_{7/2}d_{5/2})$ neutrons to less than their maximal value; in this case the nine neutrons couple to $I=(19/2)\hbar$ rather than their maximum of $(23/2)\hbar$. The higher spin of the final terminating state at $I^\pi=99/2^+$ is generated by exciting one neutron into a $(d_{3/2}s_{1/2})$ orbital, and coupling the remaining eight $(g_{7/2}d_{5/2})$ neutrons to their maximum spin.

In the calculations, the $[2,4]^+$ configuration lies lower in energy than the $[2,4]^-$ configuration, but experimentally,

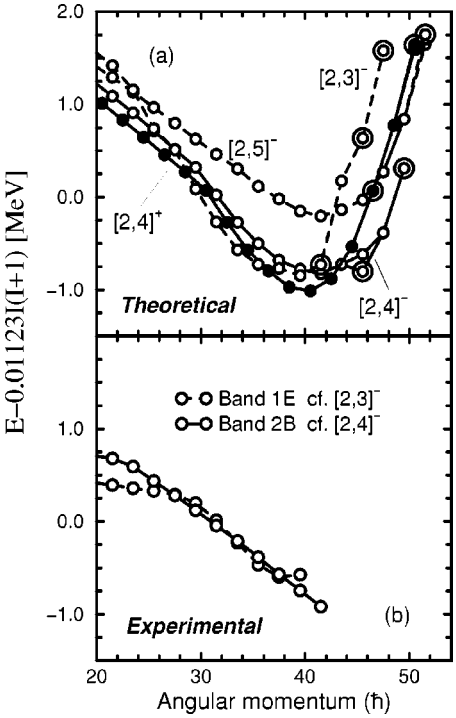

FIG. 8. The energies (a) calculated for specific configurations and (b) observed in the experimental bands, as a function of spin, shown relative to a rigid-rotor reference. The configurations are labeled by $[p,n]$ where p is the number of $h_{11/2}$ protons and n is the number of $h_{11/2}$ neutrons; the superscripts attached to the configuration labels give the sign of the total signature quantum number, α. The solid lines and dashed lines represent positive- and negative-parity configurations, respectively; similarly open and solid symbols represent positive- and negative-signature configurations. The encircled symbols in (a) represent aligned states. The three lowest configurations shown define the calculated yrast line in the spin range $I=(300-45)\hbar$. It should be pointed out that the highest data points of both bands on panel (b) are tentative.

this band (Band 2A) is not observed above $(45/2)\hbar$, suggesting that it will be higher in energy at high spin. Furthermore, while the calculated data points for the $[2,4]^-$ configuration in Fig. 8(a) show a curvature developing into a minimum, the observed Band 2B [Fig. 8(b)] is closer to a constant downward slope. In particular, the tentative $83/2^+$ state appears difficult to understand theoretically because the calculations predict that the experimental data points should start to curve upwards at these spin values, corresponding to a higher energy cost per spin unit. Band 1E shows an indication of curvature, developing at $79/2^+$, which is about $2\hbar$ earlier than predicted by the calculations.

In a similar way, the pronounced upslope (Fig. 8) caused by the tentatively observed $79/2^-$ state in Band 1E is difficult to understand from the calculations. On the other hand, it should be noted that this is a region where neutron $(g_{7/2}d_{5/2})$ and $(d_{3/2}s_{1/2})$ orbitals are expected to compete in energy as discussed above and in more detail in Ref. [41]. Depending on the exact relative positions of these orbitals, different discontinuities might be expected.

V. SUMMARY

In summary, excited states have been identified in ^{119}Ba and observed to high spins despite the small production cross sections involved. Two rotational bands have been identified, which are most likely based on the $\nu(h_{11/2})[532]5/2^-$ and $\nu(g_{7/2}d_{5/2})[413]5/2^+$ orbitals, and which extend to spins of $(75/2)\hbar$ and $(79/2)\hbar$, respectively. The low-spin quasiparticle alignments can be explained well, and the two bands are in excellent agreement with the excitation-energy systematics. This is the most-neutron-deficient odd-A barium isotope in which excited states have been identified, yet states have been observed to about $6\hbar$ higher in spin than any other odd-A barium isotope. The aligned angular momenta of the bands are partially explained using standard cranked Woods-Saxon calculations. The alignment of the first pair of $h_{11/2}$ protons is observed in both bands, and there is some evidence for $h_{11/2}$ neutron alignments. At higher spins, the expected quasiparticle alignments are not observed, which may be because nucleons are aligning continuously as described in the mechanism of smooth band termination. Configuration-dependent cranked Nilsson-Strutinsky calculations reproduce the experimental data reasonably well, suggesting that smooth band termination effects are important at the highest spins. The bands are observed to within a few spin units of the predicted terminating spins. In a future experiment, it will be interesting to study these bands to higher spins, in order to test whether they do indeed terminate. The observation of smooth band termination at $Z=56$ would demonstrate a widespread applicability of the phenomenon.

ACKNOWLEDGMENTS

The authors would like to thank A. Lipski for target preparation and E.S. Paul for useful discussions. The CSM and TRS codes were provided by R. Wyss and W. Nazarewicz. This work was supported in part by the NSF, by the EPSRC (U.K.), by the Department of Energy, Nuclear Physics Division, under Contract Nos. W-31-109-ENG-38 (ANL) and DE-AC03-76SF00098 (LBNL), and by the Swedish Natural Science Research Council. A.V.A. would like to acknowledge support from the Alexander von Humboldt Foundation.

[1] J.F. Smith *et al.*, Phys. Rev. C **57**, R1037 (1998).
[2] W. Urban *et al.*, Nucl. Phys. **A613**, 107 (1997).
[3] F. Lidén, L. Hildingsson, Th. Lindblad, J. Gizon, D. Barnéoud, and J. Gascon, Nucl. Phys. **A524**, 141 (1991).
[4] B. Cederwall, A. Johnson, R. Wyss, C.G. Lindén, S. Mitarai, J. Mukai, B. Fant, S. Juutinen, P. Ahonen, and J. Nyberg, Nucl. Phys. **A529**, 410 (1991).
[5] R. Wyss, F. Lidén, J. Nyberg, A. Johnson, D.J.G. Love, A.H. Nelson, D.W. Banes, J. Simpson, A. Kirwan, and R. Bengtsson, Z. Phys. A **330**, 123 (1988).
[6] J.P. Martin, V. Barci, H. El-Samman, A. Gizon, J. Gizon, W. Klamra, B.M. Nyako, F.A. Beck, Th. Byrski, and J.C. Merd-

inger, Nucl. Phys. **A489**, 169 (1988).
[7] D. Ward, H.R. Andrews, V.P. Janzen, D.C. Radford, J.K. Johansson, D. Prévost, J.C. Waddington, A. Galindo-Uribarri, and T.E. Drake, Nucl. Phys. **A539**, 547 (1992).
[8] A.P. Byrne, K. Schiffer, G.D. Dracoulis, B. Fabricius, T. Kibédi, A.E. Stuchberry, and K.P. Lieb, Nucl. Phys. **A548**, 131 (1992).
[9] R. Wyss *et al.*, Nucl. Phys. **A505**, 337 (1989).
[10] A. Granderath, P.F. Mantica, R. Bengtsson, R. Wyss, P. von Brentano, A. Gelberg, and F. Seiffert, Nucl. Phys. **A597**, 427 (1996).
[11] A.V. Afanasjev, G.J. Lane, D.B. Fossan, and I. Ragnarsson, Phys. Rep. **322**, 1 (1999).
[12] I. Ragnarsson, V.P. Janzen, D.B. Fossan, N.C. Schmeing, and R. Wadsworth, Phys. Rev. Lett. **74**, 3935 (1995).
[13] V.P. Janzen *et al.*, Phys. Rev. Lett. **72**, 1160 (1994).
[14] R. Wadsworth *et al.*, Phys. Rev. Lett. **80**, 1174 (1998).
[15] R. Wadsworth *et al.*, Phys. Rev. C **50**, 483 (1994).
[16] R. Wadsworth *et al.*, Phys. Rev. C **53**, 2763 (1996).
[17] H. Schnare *et al.*, Phys. Rev. C **54**, 1598 (1996).
[18] G.J. Lane *et al.*, Phys. Rev. C **55**, R2127 (1997).
[19] G.J. Lane *et al.*, Phys. Rev. C **58**, 127 (1998).
[20] I. Thorslund *et al.*, Phys. Rev. C **52**, R2839 (1995).
[21] M.P. Waring *et al.*, Phys. Rev. C **51**, 2427 (1995).
[22] H.C. Scraggs *et al.*, Nucl. Phys. **A640**, 337 (1998).
[23] J.M. Sears, D.B. Fossan, G.R. Gluckman, J.F. Smith, I. Thorslund, E.S. Paul, I.M. Hibbert, and R. Wadsworth, Phys. Rev. C **57**, 2991 (1998).
[24] P.J. Nolan, F.A. Beck, and D.B. Fossan, Annu. Rev. Nucl. Part. Sci. **45**, 561 (1994).
[25] C.N. Davids *et al.*, Nucl. Instrum. Methods Phys. Res. B **40/41**, 1224 (1989); C.N. Davids *et al.*, *ibid.* **70**, 358 (1991).
[26] J.F. Smith *et al.*, Phys. Lett. B **406**, 7 (1997).
[27] D.C. Radford, Nucl. Instrum. Methods Phys. Res. A **361**, 297 (1995); D.C. Radford, *ibid.* **361**, 306 (1995).
[28] F. Lidén *et al.*, Nucl. Phys. **A550**, 365 (1992); R. Wadsworth *et al.* (unpublished).
[29] S. Törmanen *et al.*, Nucl. Phys. **A572**, 417 (1994); E.S. Paul, D.B. Fossan, K. Hauschild, H. Schnare, J.M. Sears, I. Thorslund, R. Wadsworth, A.N. Wilson, and J.N. Wilson, Phys. Rev. C **51**, R2857 (1995).
[30] S. Pilotte *et al.*, Nucl. Phys. **A514**, 545 (1990).
[31] P. Möller, J.R. Nix, W.D. Myers, and W.J. Swiatecki, At. Data Nucl. Data Tables **59**, 185 (1995).
[32] S.A. Wells, D.E. Evans, J.A.R. Griffith, D.A. Eastham, J. Groves, J.R.H. Smith, D.W.L. Tolfree, D.D. Warner, J. Billowes, I.S. Grant, and P.M. Walker, Phys. Lett. B **211**, 272 (1988).
[33] D.D. Bogdanov, I. Voborzhil, A.V. Dem'yanov, V.A. Karnaukhov, O.K. Nefed'ev, and L.A. Petrov, Sov. J. Nucl. Phys. **24**, 4 (1976).
[34] R. Bengtsson and S. Frauendorf, Nucl. Phys. **A327**, 139 (1979).
[35] S.M. Harris, Phys. Rev. **138**, B509 (1965).
[36] R. Wyss, J. Nyberg, A. Johnson, R. Bengtsson, and W. Nazarewicz, Phys. Lett. B **215**, 211 (1989).
[37] W. Nazarewicz, G.A. Leander, and A. Johnson, Nucl. Phys. **A503**, 285 (1989).
[38] W. Nazarewicz, J. Dudek, R. Bengtsson, and I. Ragnarsson, Nucl. Phys. **A435**, 397 (1985).
[39] S. Cwiok, J. Dudek, W. Nazarewicz, W. Skalski, and T. Werner, Comput. Phys. Commun. **46**, 379 (1987).
[40] A.V. Afanasjev and I. Ragnarsson, Nucl. Phys. **A591**, 387 (1995).
[41] A.V. Afanasjev and I. Ragnarsson, Nucl. Phys. **A628**, 580 (1998).